RMetS
Royal Meteorological Society

Tropical low formation and intensification over land as seen in ECMWF analyses

Gerard Kilroy,[a]* Roger K. Smith[a] and Michael T. Montgomery[b]
[a]*Meteorological Institute, Ludwig-Maximilians University of Munich, Germany*
[b]*Department of Meteorology, Naval Postgraduate School, Monterey, CA, USA*

*Correspondence to: G. Kilroy, Meteorological Institute, Ludwig-Maximilians University of Munich, Theresienstr. 37, 80333 Munich, Germany. E-mail: gerard.kilroy@lmu.de

Case studies of the formation and intensification over land of three tropical lows in northern Australia are described. The case studies are based on European Centre for Medium-Range Weather Forecasts (ECMWF) analyses. The aim is to investigate the generality of recent results concerning the dynamics and thermodynamics of tropical lows. Consistent with these results, it is found that the processes of low formation and intensification are the same over land as over the ocean. An important element of the intensification process is the need for bursts of deep convection to persist near the circulation centre, which, in turn, requires that convective instability be maintained by surface moisture fluxes. The moist monsoonal environment locally surrounding the storm provides a shield against the adverse effects of dry-air intrusion from the Australian continent.

Key Words: tropical depressions; tropical lows; tropical cyclogenesis; monsoonal lows

Received 16 June 2016; Revised 27 September 2016; Accepted 2 November 2016; Published online in Wiley Online Library

1. Introduction

The Australian 'wet season' (November–April) is characterized by a trough of low pressure that lies south of the Equator. At the beginning of the wet season, this monsoon trough lies to the north of the Australian continent, but later it moves southwards, sometimes lying over the continent. At such times it is common for tropical lows to develop over land somewhere along the trough. We use the term tropical low to describe a non-frontal, warm-core vortex with cyclonic flow at the surface and with embedded moderate or deep moist convection to distinguish it from a dry heat low. Occasionally, a low may form close enough to the coast to be of particular concern to forecasters, since if the low moves over the sea it has a strong chance of developing into a tropical cyclone. Even if the low remains over land, or if it forms over the sea and moves over the land (sometimes as a land-falling tropical cyclone), it can produce heavy rainfall and serious flooding over a large area. An important landmark study of tropical cyclogenesis during the Australian monsoon is that of McBride and Keenan (1982).

Even when the lows form over land, they do so where there is relatively sparse conventional data coverage and, until recently, little was known about their formation mechanism or their structure. One of the most important questions from a forecasting perspective is whether or not a low will develop in the forecast area, and when. While answering the last question would inevitably require the use of guidance from numerical forecast systems, an improved understanding of the basic mechanisms would be helpful.

Seminal studies by Hendricks *et al.* (2004), Montgomery *et al.* (2006), Nolan (2007), Dunkerton *et al.* (2009) and Raymond and López Carillo (2011) have led to important advances in understanding maritime tropical cyclogenesis. The first two studies suggested the important role of rotating deep convection in the formation process, while that of Dunkerton *et al.* highlighted the nurturing role of a tropical wave and provided a new framework for understanding how such hybrid wave–vortex structures develop into tropical lows. These and related work by Tory *et al.* (2006a, 2006b, 2007) in relation to tropical cyclogenesis in the Australian region are summarized by Smith *et al.* (2015), together with two earlier studies relevant to this region by Foster and Lyons (1984) and Davidson and Holland (1987). The Tory *et al.* studies raise the question as to whether the development of monsoon lows over land is fundamentally different from the genesis of tropical cyclones over the sea.

With a view to answering this question, Smith *et al.* (2015) investigated the formation of three lows that developed on the Australian monsoon shear line during January 2013 on the basis of European Centre for Medium-Range Weather Forecasts (ECMWF) analyses. Interpretations of their formation were given in terms of vorticity dynamics. Two of these lows eventually became tropical cyclones and their formation was distinguished by persistent bursts of (parametrized) deep convection that occurred near the circulation centre.

A similar analysis for a tropical low that formed near Darwin, Australia in January 2014 was carried out by Kilroy *et al.* (2016), again based on ECMWF analyses. This low intensified over land as it tracked southwards, away from the coast. Kilroy *et al.* investigated the moisture budget for this event also. The budget was performed over square columns of area 2°lon × 2°lat, 4°lon × 4°lat and 6°lon × 6°lat that moved with the low. For this purpose, the low centre was defined by the location of minimum

geopotential at 850 mb. It was found that the horizontal transport of moisture into a column was comparable with the moisture lost by precipitation and that the surface flux of moisture was small in comparison. Nevertheless, it was argued that, although proportionately small, the surface moisture flux is needed to maintain conditional instability near the vortex centre and thereby to ensure that bursts of deep convection can continue to occur near the circulation centre. Similar results were found in a convection-permitting numerical study of a different monsoonal low that developed over land in the same region of Australia by Tang *et al.* (2016).

Consistent with the analyses of Smith *et al.* (2015), those by Kilroy *et al.* (2016) and Tang *et al.* (2016) indicated that the intensification of a tropical low requires the occurrence of repeated bursts of deep convection occurring near the circulation centre. From a vorticity perspective, the convectively induced lower-tropospheric convergence acts to concentrate cyclonic vorticity near the circulation centre, leading to an enhancement of the local circulation about the centre. In turn, the increase in circulation corresponds with an increase in the local tangential wind speed. Assuming approximate gradient wind balance above the boundary layer, there would be a corresponding fall in central pressure. This feature was highlighted in convection-permitting sensitivity experiments by Tang *et al.* (2016), who found that deep convective bursts near the circulation centre were invariably accompanied by pulses of intensification.

1.1. *The present study*

As a further step to developing a basic conceptual model of tropical lows over land and to examine the generality of recent findings discussed above, we have undertaken case studies of three further events, all of which intensified while over land and provided a particular challenge to local forecasters. The case studies are based on certain kinematic, dynamic and thermodynamical fields extracted from ECMWF analyses.

The article is organized as follows. In section 2 we summarize the data used for the study and introduce the three cases to be analyzed. The three subsequent sections present the analyses of each case. There follows a section synthesizing the findings from these events and finally a section detailing the conclusions.

2. Data, cases and methodology

The ECMWF analyses used here are obtained from a global 4DVAR analysis and prediction system (see e.g. Bauer *et al.*, 2011). Forecasters consider the predictions from the ECMWF system to be as good as any available. The analyses are available at the surface and at 21 or 25 pressure levels between 1000 and 1 mb (the number of pressure levels was increased from 21 to 25 on 6 November 2007). The analyses are available at 6 h intervals. The data cover the domain from 100°E to 160°E and from the Equator to 30°S, with a horizontal grid spacing of 0.125°. The case studies are based on selected kinematic, dynamic and thermodynamical fields extracted from these analyses.

Three cases are chosen here for investigation: the unnamed tropical low that formed near Darwin in January 2006 during the Tropical Warm Pool International Cloud Experiment (TWP-ICE: see May *et al.* 2008a, 2008b); the low that became Severe Tropical Cyclone *George* in February 2007; and the low that became Tropical Cyclone *Carlos* in February 2011. Interest is confined to the early stages of formation while the systems are centred over land. A numerical simulation of the 2006 unnamed low is discussed in a recent article by Tang *et al.* (2016).

As in Smith *et al.* (2015) and Kilroy *et al.* (2016), our interpretations of low formation are based on vorticity dynamics. While vertical vorticity is useful for characterizing local rotation, it may be associated also with regions of significant horizontal shear deformation, which are detrimental to the formation of concentrated vortices. Regions where the vorticity is dominated by rotation are more favourable for vortex development than those dominated by strain. For this reason, we also analyze the Okubo–Weiss (OW) parameter (Dunkerton *et al.*, 2009; see also the section 'Vorticity and Okubo–Weiss diagnostics' and the appendix of Smith *et al.*, 2015) to highlight regions where the flow is dominated by rotation. Such regions are ones where patches of enhanced vertical vorticity congeal most easily to form a monopole structure.

As in Kilroy *et al.* (2016), we examine also a moisture budget for a mesoscale column of air (from the surface to the model top). The budget may be written as

$$\frac{\partial Q}{\partial t} = E - P + MC, \tag{1}$$

where $\partial Q/\partial t$ is the time change in total precipitable water, E is the rate of surface evaporation of moisture, P is the rate of moisture loss by precipitation and MC is the rate of moisture convergence. Precipitation and evaporation are variables available in the ECMWF forecast data, while moisture convergence is calculated by vertically integrating the fluxes of moisture into a column centred on the system. These quantities are averaged over the area of the column and have units of kg s^{-1} m^{-2}. Some issues regarding closure in the moisture budget are discussed in Kilroy *et al.* (2016).

3. The unnamed low of January 2006

This tropical low formed off the north coast of the Top End* around 0000 UTC† on 22 January. Figure 1 shows the subsequent track, together with the evolution of the intensity and magnitude of the vertical wind shear. The vertical shear is calculated as the magnitude of the vector velocity difference between 850 and 200 mb averaged over columns with cross-sections 2°lon×2°lat, 4°lon × 4°lat and 6°lon×6°lat centred on the location of minimum geopotential at 850 mb.‡ The intensity is characterized by the maximum wind speed at 850 mb within the 2°lon × 2°lat column.

During the first few days shown, the low moved northwards and then westwards and strengthened in an environment of moderate ($\approx 10\,\mathrm{m\,s^{-1}}$) vertical shear, making landfall in the Darwin area around 1800 UTC on 24 January. Thereafter it drifted southwards along the western border of the Northern Territory and weakened. Coincident with a weakening of the shear from 1200 UTC on 25 January, the low re-intensified and around 0000 UTC 26 January it began to track southeastwards, reaching a maximum intensity of about $30\,\mathrm{m\,s^{-1}}$ at 1800 UTC on 27 January. From 0000 UTC on 29 January, the low gradually weakened while moving southwestwards. The low heralded an active monsoon onset over the northern Top End, which brought heavy rainfall to many parts of the western Northern Territory.

Figure 2 shows the wind structure at 850 mb, together with the wind vectors and contours of zonal wind component and geopotential height at 0000 UTC on 21, 23, 25 and 27 January 2006. On 21 January, the wind field is dominated by Tropical Cyclone *Daryl*, located near 117°E, 20°S. There is a weak geopotential low located over the Gulf of Carpentaria, although at this time there is no noticeable circulation associated with the low. By 0000 UTC on 23 January (b), the large-scale flow has changed dramatically, with a strengthening of the westerlies north

*'Top End' refers loosely to the northernmost section of the Northern Territory of Australia, bounded by the Joseph Bonaparte Gulf on the western side and the Gulf of Carpentaria on the eastern side.

†Note that local time is 9.5 h ahead of UTC (Universal Time Coordinated).

‡As in our earlier studies, we compute first the local vector velocity difference and then compute the average over the column. Because of the linearity of the shear vector calculation, the method is equivalent to computing the vector shear from the difference in the areal average velocity at the two levels. This is equivalent to the method adopted by DeMaria and Kaplan (1994, p. 213) as a basis for their Statistical Hurricane Intensity Prediction Scheme (SHIPS).

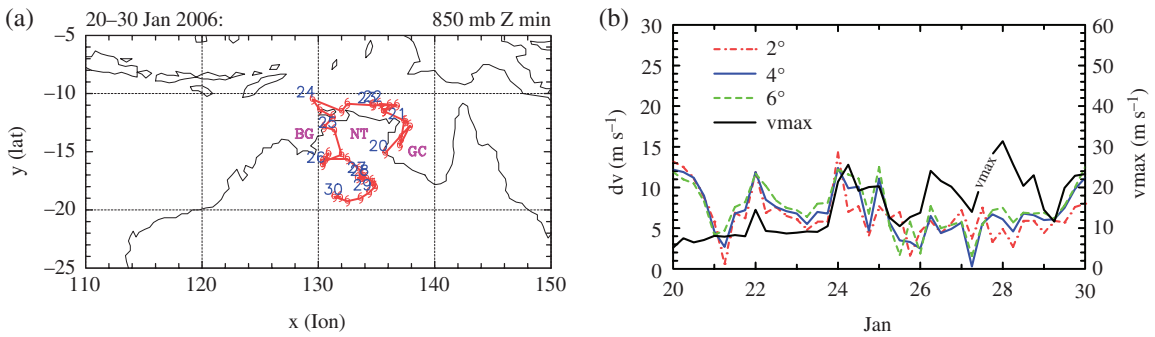

Figure 1. (a) Track of the Northern Territory tropical low: 20–30 January 2006. Positions of minimum geopotential at 850 mb are indicated by cyclone symbols every 6 h. Positions at 0000 UTC are shown by date. Shown also are the locations of the Northern Territory (NT), the Bonaparte Gulf (BG) and the Gulf of Carpentaria (GC). (b) Mean vertical wind shear, characterized by the magnitude of the vector velocity difference between 850 and 200 mb, averaged over mesoscale columns 2°lon × 2°lat, 4°lon × 4°lat and 6°lon × 6°lat centred on the location of minimum geopotential at 850 mb and maximum wind speed (v_{max}) at 850 mb within the 2°lon × 2°lat column.

of Darwin, the development of a broad circulation over the Top End and a fall of 850 mb geopotential height near the centre of this circulation. At this time, the low centre is located just north of the coastline. By 0000 UTC on 25 January (c), the geopotential low is centred over land, essentially above Darwin, but has not deepened, although the region of strong westerlies has increased in areal extent. In the following 48 h, the system moves southwards over land, intensifying as it does so (d). From 25 January onwards, the magnitude of the vertical shear decreases and, despite being located over land, the low continues to strengthen. A key feature to note is that the easterlies to the south of the system remain mostly weak throughout the period shown in Figure 2, in contrast to the systems described in Smith *et al.* (2015) and Kilroy *et al.* (2016).

Figure 3 provides a vorticity and OW perspective of the foregoing development. Shown are the vertical component of absolute vorticity, the corresponding wind vectors, the contours of geopotential height at 850 mb and the distribution of the OW parameter at 850 mb at 0000 UTC on 23 January, 25 January and 27 January. At 0000 UTC on 23 January, the most striking feature in the absolute vorticity field is the extensive region of elevated cyclonic values[§] to the north of the Top End. Centred over this region is a weak cyclonic vortex circulation, within which is a coherent region of positive OW values. The latter region is coherent up to 500 mb (not shown), an indicator of the potential for further vortex development. At 0000 UTC on 25 January, the areal extent of both the cyclonic vertical vorticity and OW regions has decreased. By 0000 UTC on 27 January, the system has intensified further, although the size of the regions of enhanced cyclonic vertical vorticity and OW remains relatively small compared with the events discussed in Smith *et al.* (2015) and Kilroy *et al.* (2016). A reduction in the areal extent of the positive OW region would be detrimental to deep convection around the periphery of the vortex, reducing the ability of such clouds to induce inflow and converge vorticity.

To illustrate the role of deep convection in the evolution of low-level vorticity, we portray areas of strong vertical velocity (vertical p velocity, $\omega < -2.0\,\mathrm{Pa\,s^{-1}}$) at 500 mb, which are a proxy for regions of deep convection in the analyses. The vertical velocity fields at 0000 UTC on 24 and 25 January are shown in Figure 4 with the horizontal wind fields at 850 mb superimposed. On 24 January, strong vertical motion (indicated by the yellow contours in Figure 4(a)) occurs near the centre of the circulation. Following this 'pulse' of deep convection, the low has a larger maximum wind speed (see Figure 1(b)). On 25 January at 0000 UTC, there is a region of marked subsidence near the vortex centre and there is a subsequent reduction in the maximum wind speed at this time (see Figure 1(b)).

[§]For plotting, the sign of the vertical vorticity is reversed so that cyclonic vorticity is positive.

Shown in Figure 5 are time–height cross-sections of several quantities averaged over a square column of 2°lon × 2°lat centred on the minimum geopotential at 850 mb. These quantities are the vertical mass flux (approximated by $-\omega/g$), the temperature deviation from the column-averaged temperature at the start of the time series at all heights, the relative humidity and the pseudo-equivalent potential temperature, θ_e. The figure shows also a time–height cross-section of the circulation around the column and the moisture budget for the column (the method for calculating this budget is given by Kilroy *et al.*, 2016). The circulation is defined as the line integral of the horizontal velocity vector around the boundary of the column at any pressure level. This quantity is normalized by the length of the boundary.

Noteworthy features in Figure 5(a) are two 'bursts' of deep convection on 24 January and one at about 1800 UTC on 27 January. The first two bursts are accompanied by a decrease in the magnitude of vertical shear within the column and an increase in the maximum tangential wind speed (see Figure 1(b)). Not surprisingly, these bursts are seen as sharp peaks in precipitation. They are accompanied also by a prominent increase in the moisture flux into the column, which is associated with the low-level convergence induced by convection (Figure 5(b)). The relative humidity averaged over the column (Figure 5(d)) does not indicate any appreciable intrusion of dry air into the inner core of the vortex.

As in the tropical low examined by Kilroy *et al.* (2016), the total moisture supply to the system is dominated by the convectively induced import of moisture into the sides of the column, while the contribution from surface moisture fluxes is comparatively small. The moist monsoonal environment locally surrounding the storm provides a shield against the adverse effects of dry-air intrusion from the Australian continent. Of course, as noted by Kilroy *et al.* (2016) and Tang *et al.* (2016), the presence of plentiful column moisture, by itself, does not guarantee the occurrence or prolongation of deep convection. Deep convection depends on the existence of conditional instability and sustained deep convection requires that this instability be continually renewed. Thus, even though surface moisture fluxes make only a small contribution to the moisture budget, they are essential for vortex intensification by maintaining conditional instability in the inner region of the vortex. Evidence for this maintenance is provided by periodic increases in low-level θ_e discussed below.

In terms of surface latent heat flux, the daytime values at 0000 UTC on 22–28 January averaged over the 2°lon × 2°lat square column are 157, 123, 245, 231, 103, 114 and 99 W m^{-2}, respectively, and those at 1200 UTC on these days are 71, 101, 118, 17, 28, 32 and 23 W m^{-2}, respectively. Note that the system moves over land at about 1800 UTC on 24 January. Unfortunately, the fluxes are available at only 12 h intervals, so it is not possible to determine a reliable 24 h mean.

Following the convective bursts on 24 January, there are several periods when the precipitation inside the column is nearly zero.

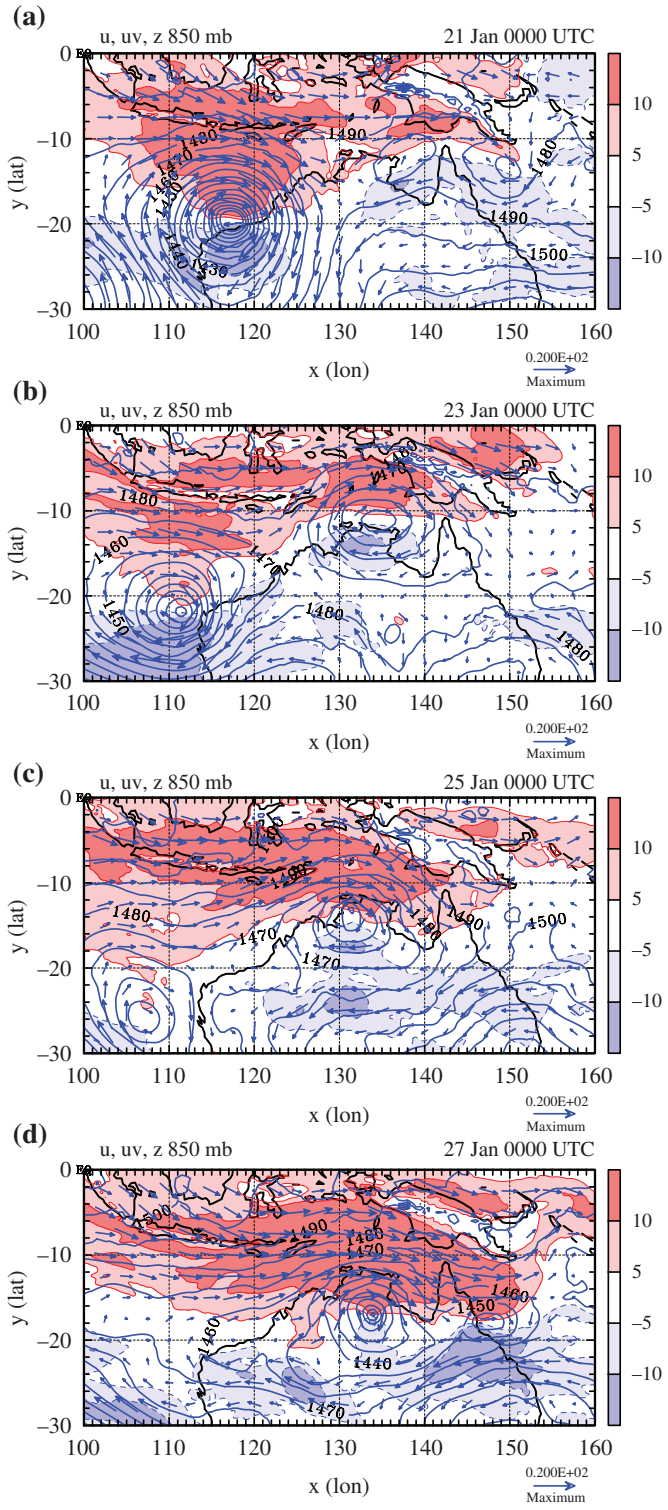

Figure 2. Wind vectors at 850 mb, together with contours of the zonal wind component and geopotential height at 0000 UTC on (a) 21 January, (b) 23 January, (c) 25 January and (d) 27 January 2006, illustrating the formation of the Northern Territory low. The westerly wind component greater than 5 m s^{-1} is shaded pink, that greater than 10 m s^{-1} is shaded red. Easterly winds greater than 5 m s^{-1} in magnitude are shaded light blue, those greater than 10 m s^{-1} in magnitude are shaded blue. The contour interval for geopotential height is 10 m. Solid contours are positive, dashed contours negative. Wind vectors should be compared with the reference vector (20 m s^{-1}) at the bottom right of each panel.

At 0000 UTC on 25 January, the lateral moisture flux into the column is negative (Figure 5(b)), a feature that is presumably associated with subsidence within the column, and the Total Precipitable Water (TPW) is lower than earlier. The brief period of marked subsidence on 25 January at 0000 UTC (Figure 5(a)) is accompanied by a decrease in both the mid-level relative humidity and θ_e, but the system slowly recovers, with a progressive elevation of mid-level θ_e over the 10 day period shown. There are periodic increases in low-level θ_e as well. These are likely to be associated with surface moisture fluxes and indicate maintenance of convective instability in the column. During this same period, there is a general warming of the middle and upper troposphere, but cooling in the lower troposphere, mostly below 900 mb and greater than 1 °C in magnitude. The warming is presumably associated with latent heat release in convection and the cooling with convectively induced mesoscale downdraughts. However, it is not possible to confirm these suppositions from the data available in the analyses. This is a topic that merits further study.

The circulation around the column remains relatively weak until the second convective burst at 1800 UTC on 27 January (Figure 5(f)). At this time, the system is far inland (Figure 1(a)). Perhaps significantly, the largest circulation at any one time is found in the lower troposphere, typically at pressures above 800 mb (i.e. altitudes below 2 km).

In summary, in the presence of an environment of moderate vertical shear, the early intensification of the unnamed low of January 2006 was slow. Then, following a day of sustained convection that occurred close to the circulation centre, the mean vertical shear reduced and the low intensified while over land. As noted by Kilroy *et al.* (2016), it is not possible to attribute the intensification to the decrease in vertical shear: it may have been that the intensification itself led to the reduction in vertical shear.

4. Formation of Tropical Cyclone *George* (2007)

Severe Tropical Cyclone *George* was reported to be the most destructive cyclone to affect Western Australia since Tropical Cyclone *Joan* in 1975. Figure 6(a) shows the track of the cyclone and its precursor low during the period of interest: 27 February–9 March. The cyclone was named on 3 March while over the Joseph Bonaparte Gulf and it became a Severe Tropical Cyclone (Category 3) on the evening of 7 March. Interest is focused here on the formation of its precursor disturbance over the Top End of Australia.

As in Figure 1(b), Figure 6(b) shows the maximum wind speed at 850 mb within the 2°lon × 2°lat column centred on the minimum geopotential at 850 mb. It shows also the magnitude of the mean vertical wind shear between 850 and 200 mb over various mesoscale columns. From early on, even in the presence of moderate to strong vertical wind shear (≈10–15 m s^{-1}), the precursor to *George* has a relatively large maximum wind speed (about 25 m s^{-1}). This maximum is more a reflection of the relatively strong environmental westerlies than the strength of the disturbance itself. On 0000 UTC on 3 March, the vertical wind shear decreases sharply in magnitude (to less than 5 m s^{-1}) and the system intensifies over water to a tropical cyclone.

Shown in Figure 7 are the wind vectors at 850 mb together with the contours of the zonal wind component and geopotential height at 0000 UTC on 27, 28 February and 2, 4 March 2007. On 27 February, the wind field is dominated by strong westerlies north of 10°S and strong widespread easterlies over much of continental Australia. There are two low-pressure systems present at this time, one located over the Top End of the Northern Territory and the other located over the ocean northeast of Australia. We focus our interest on the system located over the Top End, which develops into Tropical Cyclone *George*. At this time there is no noticeable circulation associated with the low, although the maximum wind speed is relatively large (Figure 6), a reflection of the strong monsoonal flow.

On 28 February, the low has deepened considerably and there is a noticeable circulation associated with it. Two days later, on 2 March, the broad-scale flow is much the same, although the easterlies over the continent have weakened. On 4 March there are significant differences from 48 h earlier, with the easterlies having increased in strength over much of the continent, but the low has only deepened slightly (the 850 mb geopotential minimum decreases by 23 m). Beyond 0000 UTC on 4 March,

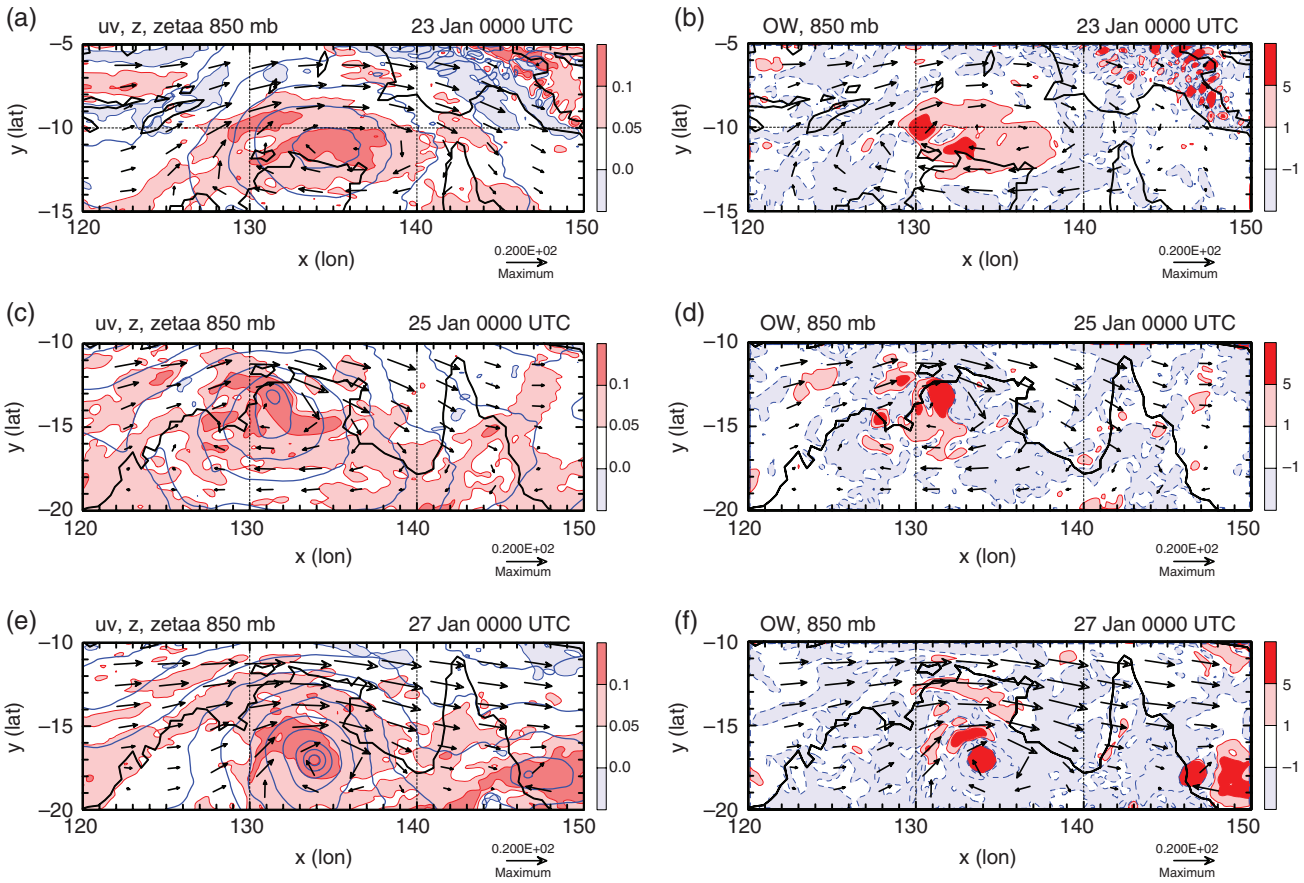

Figure 3. Left panels: wind vectors at 850 mb, together with contours of absolute vorticity (shaded) and geopotential height (thick blue contours) at 0000 UTC on (a) 23 January, (c) 25 January and (e) 27 January 2006, illustrating the formation of the low. The contour interval for geopotential height is 10 m. Absolute vorticity shading is as shown on the label bar multiplied by 10^{-3} s^{-1}. Cyclonic values of vorticity are positive (red/pink shading), anticyclonic values are negative (light blue shading). Right panels: contours of the Okubo–Weiss (OW) parameter (shaded) at 0000 UTC on (b) 23 January, (d) 25 January, and (f) 27 January 2006, illustrating the environment during the formation of the low. The contour interval for geopotential height is 10 m. OW shading is as shown on the label bar multiplied by 10^{-8} s^{-2}. Positive values have pink/red shading; negative values light blue shading. Solid contours are positive, dashed contours negative. Wind vectors should be compared with the reference vector (20 m s^{-1}) at the bottom right of each panel. Note the change in latitude range between the upper and middle/lower panels.

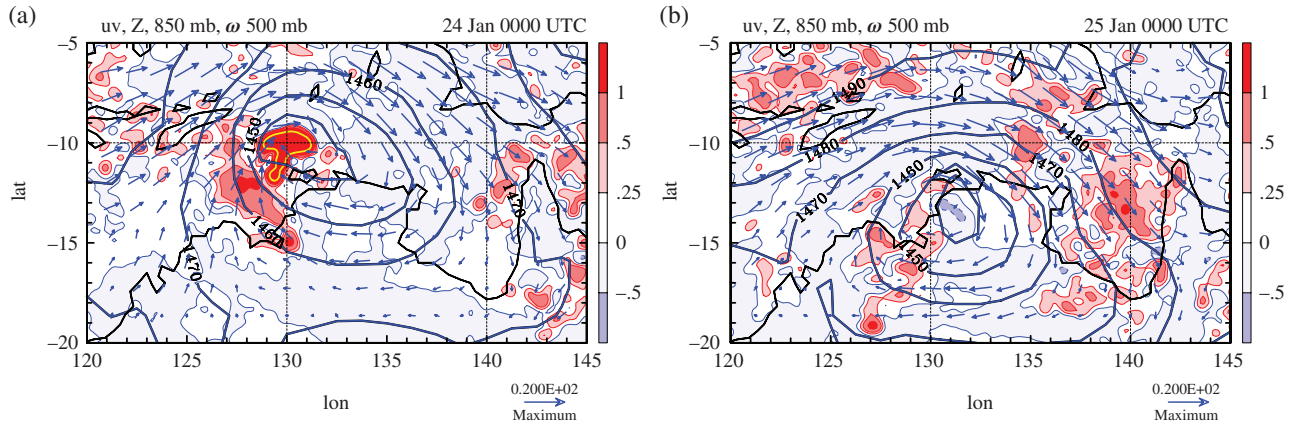

Figure 4. Wind vectors and contours of geopotential height, together with contours of the vertical velocity at 500 mb, at 0000 UTC on 24 and 25 January 2006, illustrating low formation. The contour interval for geopotential height is 10 m. The vertical p velocity ($-\omega$) shading is as shown on the label bar in units of Pa s^{-1}. Upward vertical velocities (negative values of ω) are plotted as positive (red/pink shading); negative values of vertical velocity (positive values of ω) are plotted as negative (light blue/blue shading). Strong regions of upflow are highlighted by the yellow contour (-2 Pa s^{-1}). Wind vectors should be compared with the reference vector (20 m s^{-1}) at the bottom right of each panel.

the low intensifies significantly, with the maximum wind speed reaching over 50 m s^{-1} on 7 March.

Figure 8 provides a vorticity and OW view of the foregoing development. On 27 February, the absolute vorticity field shows a broad region of elevated cyclonic values just to the immediate north of the Top End and also to the northwest and west of it. As in the case of the unnamed low, there is a coherent region near the circulation centre with strong positive OW values. Animations of the fields with 6 h output for the next 48 h suggest that the patches of elevated vertical vorticity surrounding the system are rolled up into the low centre (not shown). The region of strong positive OW persists until 1 March and is somewhat larger in size than that in the January 2006 case (compare the right panels of Figures 3 and 8).

Figure 9 shows areas of strong (as defined earlier) vertical p velocity at 500 mb, together with the wind fields at 850 mb at 0000 UTC on 27 February and 1, 3 and 4 March 2007. On 27 February there are patches of deep convection surrounding the geopotential low, although values of ω exceeding 2 Pa s^{-1} in magnitude are not present at this stage. On 3 March there are regions of strong deep convection (characterized by yellow contours) within the vortex circulation, although not within a

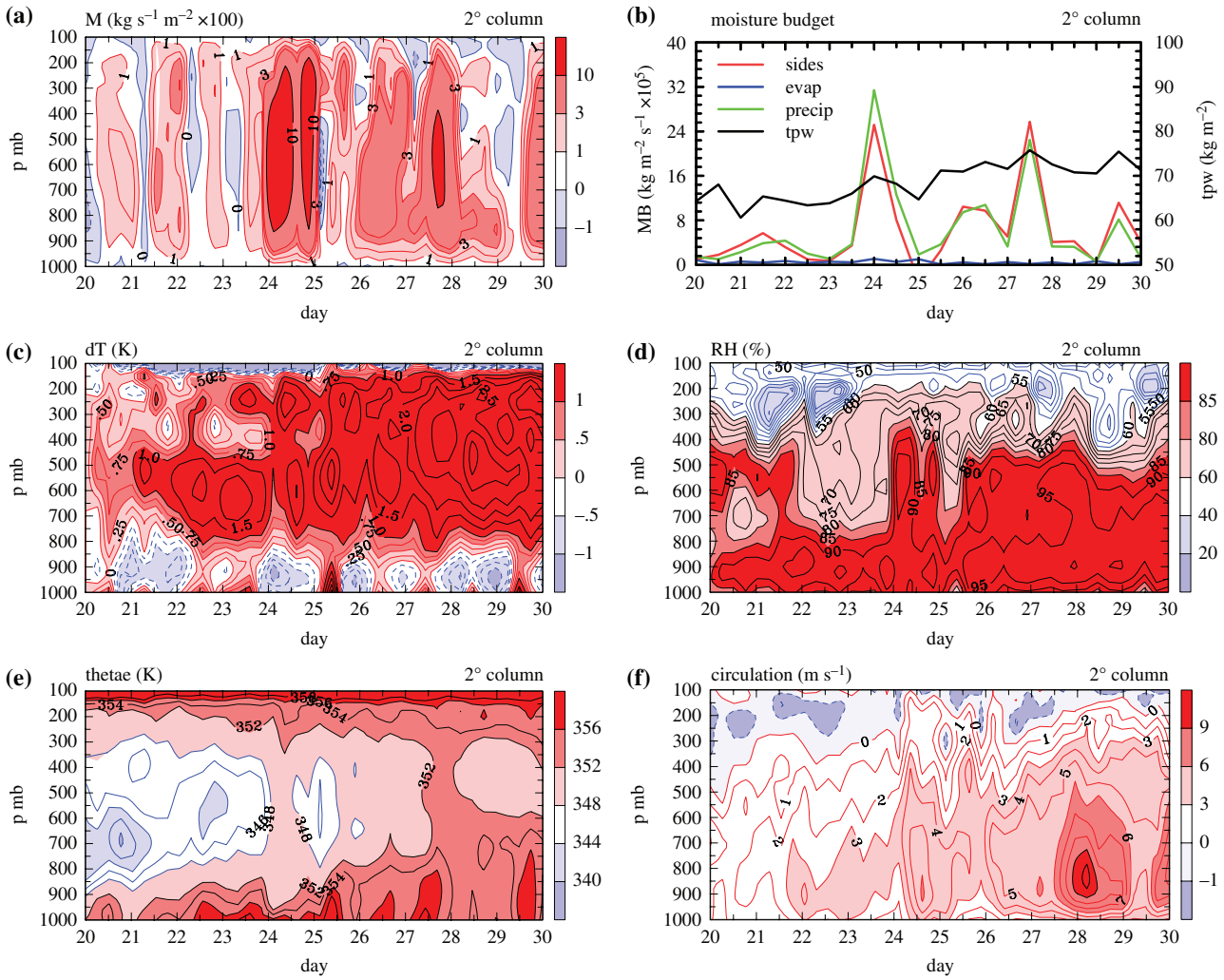

Figure 5. Time–height cross-section of system-averaged quantities within a column 2°lon × 2°lat, centred on the location of minimum geopotential at 850 mb, for the development of the unnamed low of January 2006. These include (a) the vertical mass flux per unit area, (c) the temperature deviation from that at the start of the time series, (d) relative humidity and (e) pseudo-equivalent potential temperature. Panel (f) shows the normalized circulation around the column. The circulation is normalized by the length of the boundary. Panel (b) shows the sources and sinks of moisture, including the contributions by surface evaporation, precipitation and the horizontal transport of moisture averaged over a 2°lon × 2°lat column centred on the location of minimum geopotential at 850 mb. The horizontal transport of moisture is calculated by summing the vertically integrated fluxes of moisture into the column and then dividing the sum by the area of the column, so that all terms have units of kg m $^{-2}$ s $^{-1}$. Also shown is the total precipitable water.

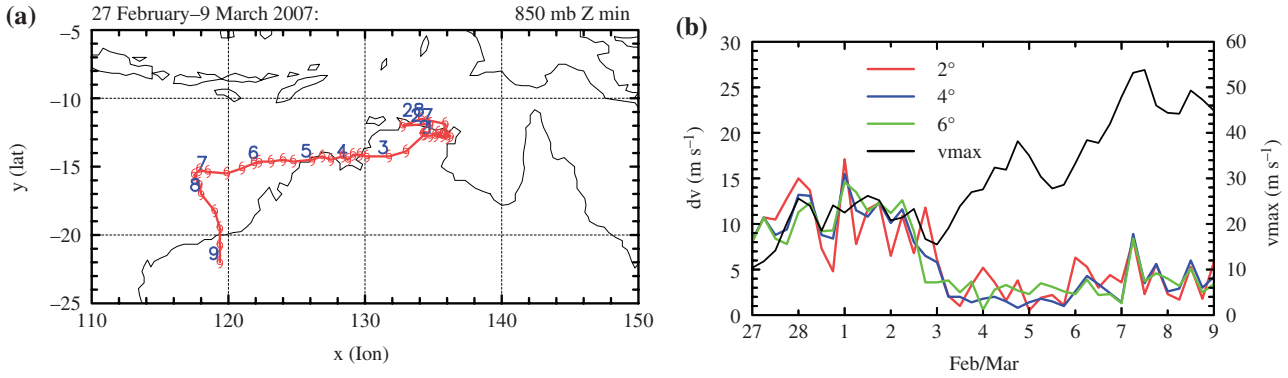

Figure 6. (a) Track of the tropical depression that developed into Tropical Cyclone *George* (2007). Positions of minimum geopotential at 850 mb are indicated by cyclone symbols every 6 h. Positions at 0000 UTC are shown by date. (b) Mean vertical wind shear, characterized by the magnitude of the vector velocity difference between 850 and 200 mb, averaged over mesoscale columns 2°lon × 2°lat, 4°lon × 4°lat and 6°lon × 6°lat centred on the location of the minimum geopotential at 850 mb and maximum wind speed at 850 mb within the 2°lon × 2°lat column.

2°lon × 2°lat column centred on the geopotential low. On 4 March the strong updraughts are located close to the circulation centre. Over the next few days, strong convection organizes near the circulation centre and the low intensifies (see below).

Figure 10 shows time–height cross-sections of column-averaged quantities as in Figure 5. Once again, prominent features are deep bursts of convection in the vertical mass flux field that occur sporadically until 4 March and then regularly afterwards.

In terms of a moisture budget, the burst on 1 March is associated with a local maximum in precipitation, although there is little precipitation within the 2°lon × 2°lat column over the next 2 days. These minima in precipitation are not found in the 4°lon × 4°lat column (not shown), suggesting that deep convection was still occurring on these days, but outside the 2°lon × 2°lat column. From 4 March onwards, bursts of deep convection, characterized by pulses of enhanced vertical mass

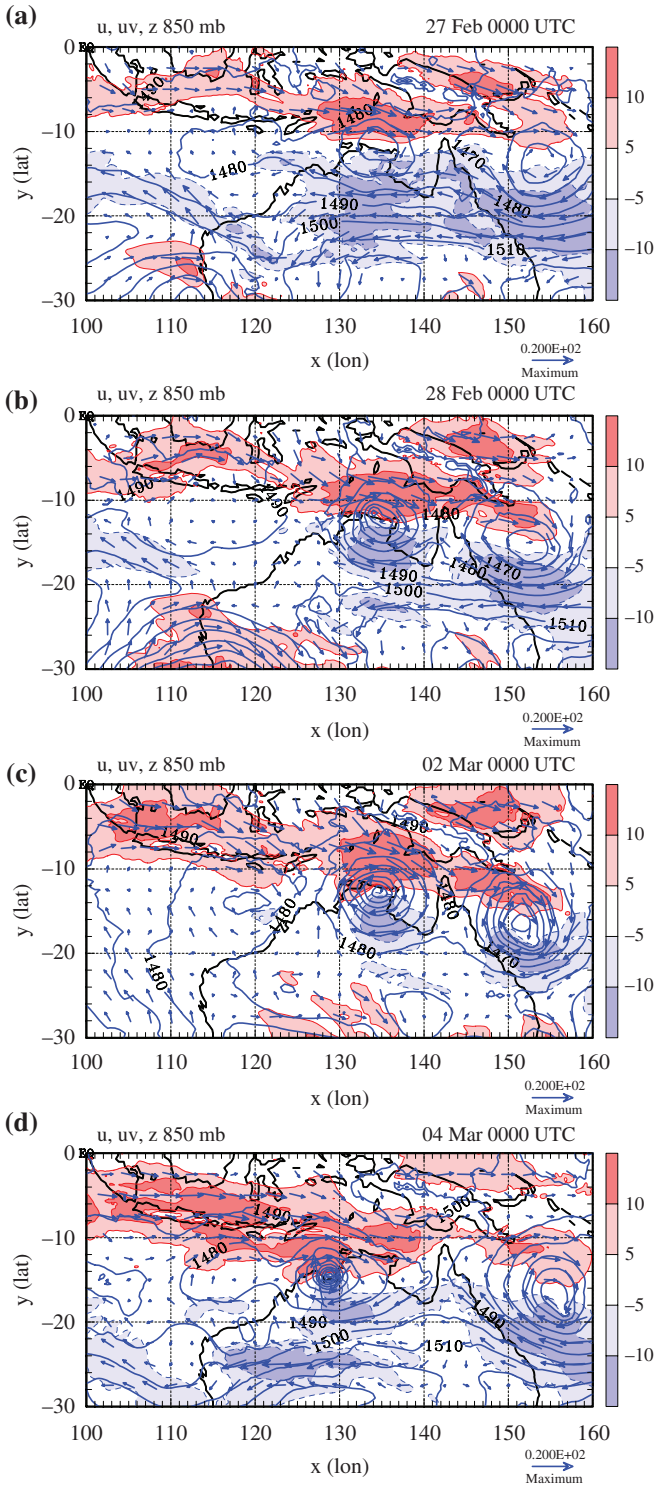

Figure 7. Wind vectors at 850 mb together with contours of the zonal wind component and geopotential height at 0000 UTC on (a) 27 February, (b) 28 February, (c) 2 and (d) 4 March 2007, illustrating the formation of the low that became Tropical Cyclone *George*. The westerly wind component greater than 5 m s^{-1} is shaded pink, while that greater than 10 m s^{-1} is shaded red. Easterly winds greater than 5 m s^{-1} in magnitude are shaded light blue, while those greater than 10 m s^{-1} in magnitude are shaded blue. The contour interval for geopotential height is 10 m. Solid contours are positive, dashed contours negative. Wind vectors should be compared with the reference vector (20 m s^{-1}) at the bottom right of each panel.

flux, occur within the 2°lon × 2°lat column. These bursts are accompanied by an increase in the flux of moisture converging into the column and also by an increase of precipitation falling out of the column.

The contribution of surface moisture fluxes increases progressively with time, reaching a maximum on 7 March at 1200 UTC, when the system lay over the sea for the second time, north of Western Australia (Figure 6). In terms of surface latent heat flux, the mean values at 0000 UTC on 3, 4 and 6 and 1200 UTC on 7 March are 126, 264, 459 and 715 W m^{-2}, respectively. Thus, typical flux values over the 2°lon × 2°lat square column are 2–5 times larger when the system is over the sea. Moreover, there is a substantial diurnal variation of the surface latent heat flux over land, with daytime values being up to four times larger than night-time values.

Note that, from a moisture-budget perspective, the moisture supply into the system is dominated by the transport of moisture into the sides of the column, even when the 2°lon × 2°lat square column lies entirely over the sea (from 1200 UTC on 5 March until 1200 UTC on 8 March).

As in the case of the unnamed low, there is a general warming of the middle and upper troposphere (Figure 10(c)), but some cooling in the lower troposphere until 6 January, when the system is well out over the sea (Figure 6(a)). We cannot explain why this cooling subsides when the system moves over the sea. In the case of Tropical Cyclone *Narelle*, discussed in Smith *et al.* (2015), there were similar features present, although the system remained over the sea for its entirety. In *George*, the relative humidity is generally high throughout the lower half of troposphere, with values mostly exceeding 85% (Figure 10(d)). As in the January 2006 case, these results do not indicate any appreciable intrusion of dry air into the inner core of the vortex. Values of mid-level θ_e are generally larger than for the unnamed low (compare Figure 10(e) with Figure 5(e)), but there is still some elevation of θ_e at low levels, except at 0000 UTC on 3 February, when the system is furthest from the coast (Figure 6(a)). At this time, there is major cooling at low levels (Figure 10(c)) and the mass-flux signature is weak at low levels (Figure 10(a)), suggesting a lull in active deep convection. Up to this time, there are again periodic increases in low-level θ_e, indicating maintenance of convective instability by surface fluxes.

The circulation around the 2°lon × 2°lat column shows a marked increase following the convective burst on 1 March, but weakens again over the next 2 days in the absence of strong deep convection within the column. Once continuous bursts of strong deep convection flare up within the column on 4 March, the circulation strengthens markedly and grows in depth. The temperature difference fields averaged over the column are very different at low levels from those in the 2006 case, with the near-surface negative anomalies much weaker in this case (compare with Figure 5(c)). As in the case of the unnamed low, the column-averaged relative humidity is generally high from the beginning of the analysis and θ_e increases steadily at all pressure levels as the system develops.

In summary, the genesis and early intensification of Tropical Cyclone *George* is different from that of the January 2006 unnamed low. The inner-core atmospheric conditions in *George* were much more favourable for intensification, with higher values of θ_e and relative humidity throughout the troposphere (compare Figure 10 with Figure 5). As the moderately strong vertical wind shear decreased in magnitude, convective bursts occurred almost continuously within the column and the vortex began to intensify, although, as noted before, we cannot establish a causal relationship between the fall in vertical wind shear and the intensification process.

5. Formation of Tropical Cyclone *Carlos* (2011)

Figure 11(a) shows the track of Tropical Cyclone *Carlos* (2011) during the period of interest, while Figure 11(b) shows time series of the mean vertical wind shear, as in Figures 1(b) and 6(b). Panel (b) shows also the maximum wind speed at 850 mb within the 2°lon × 2°lat column. At the beginning of the analysis (0000 UTC on 13 February), the magnitude of the vertical shear is small (<3 m s^{-1}), but over the next 4 days it increases in strength (with some fluctuation), reaching a maximum of about 10 m s^{-1} at 0000 UTC on 17 February.

The maximum 850 mb wind speed in the 2°lon × 2°lat column increases from less than 18 m s^{-1} to about 38 m s^{-1} over the

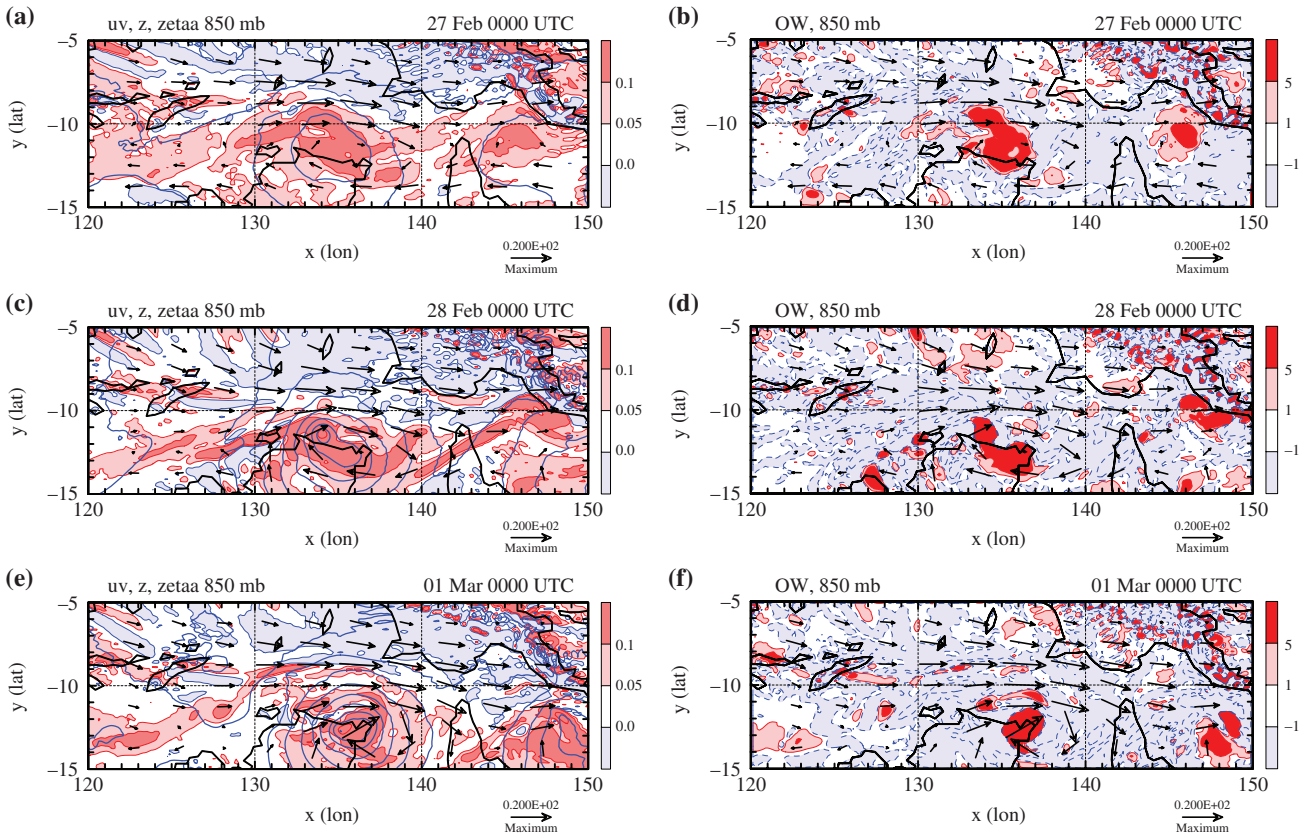

Figure 8. Left panels: wind vectors at 850 mb together with contours of absolute vorticity (shaded) and geopotential height (thick blue contours) at 0000 UTC on (a) 27 February, (c) 28 February and (e) 1 March 2007, illustrating the formation of the low that became Tropical Cyclone *George*. The contour interval for geopotential height is 10 m. Absolute vorticity shading is as shown on the label bar multiplied by 10^{-3} s^{-1}. Cyclonic values of vorticity are positive (red/pink shading), anticyclonic values are negative (light blue shading). Right panels: contours of the Okubo–Weiss (OW) parameter (shaded) at 0000 UTC on on (b) 27 February, (d) 28 February and (f) 1 March 2007, illustrating the environment during the formation of the low. The contour interval for geopotential height is 10 m. OW shading is as shown on the label bar multiplied by 10^{-8} s^{-2}. Positive values have pink/red shading, negative values light blue shading. Solid contours are positive, dashed contours negative. Wind vectors should be compared with the reference vector (20 m s^{-1}) at the bottom right of each panel.

first 3 days, before falling by 15 m s^{-1} over the next 2 days in the presence of increasing vertical wind shear. The slow-moving low was named on 16 February, but was downgraded again to a tropical low on 17 February. For the next 4 days, the system maintained its intensity despite experiencing moderate values of vertical shear. In the early hours of 21 February, the low returned to the open waters of the Indian Ocean and it re-intensified into a tropical cyclone, the 850 mb wind speed reaching a maximum of about 45 m s^{-1} on 24 February.

Figures 12(a) and (b) show the horizontal wind field and geopotential heights at 850 mb, while (c)–(f) show a vorticity and OW perspective of the low at 0000 UTC on 13 and 15 February 2011. Initially the region of strong westerlies over the northern Top End is relatively small, but over the next 48 h the westerlies increase in strength and there is a decrease in geopotential height near the circulation centre. At 0000 UTC on 13 February, there are several regions of elevated cyclonic vertical vorticity surrounding the low centre and there are strips of vorticity to the east available to be rolled up into the low (Figure 12(c)). At this time, there are only sparsely located patches of positive OW near the low centre (Figure 12(e)), suggesting that immediate development is unlikely. Over the next 48 h, a strong circulation develops, with the region of enhanced vertical vorticity consolidating further. However, regions of positive OW remain relatively small-scale compared with those in Tropical Cyclone *George* (compare Figure 12(f) with Figure 8).

We examine next the fields of 500 mb vertical p velocity. These are shown in Figure 13 at 0000 UTC on 13 and 15 February 2011, with the wind vectors at 850 mb superimposed. On 13 February, there are extensive regions of convection to the north and northeast of the geopotential low, but hardly any strong values (characterized by yellow contours) near the low centre at this time. On 15 February, there are strong values of vertical velocity near the circulation centre (Figure 13), reflecting the presence of strong deep convection. Such convection continues to occur near the circulation centre over the next few days (see Figure 14(a)).

Figure 14 shows time–height cross-sections of column-averaged quantities, as for the other cases in Figures 5 and 12. The vertical mass-flux field shows consistently high positive values ($> 3 \times 10^{-2}$ kg s^{-1} m^{-2}) throughout the troposphere from 14 February onwards, with a strong pulse late on 15 February corresponding to the local maximum in wind speed at 0000 UTC on 16 February (Figure 11(b)). From 0600 UTC on 13 February onwards, the vertical mass flux is positive and the precipitation increases in strength while the transport of moisture into the column is positive also. In general, the transport of moisture into the column and the precipitation are the dominant terms in the moisture budget, with the moisture transport slightly exceeding the precipitation at most times. The TPW in the column shows a progressive increase over the 10 day time period shown.

Surface latent heat fluxes averaged over the 2°lon × 2°lat square column have values similar to the other lows while they were over land and over the sea. For example, the values at 0000 UTC on 20 and 21 February are 106 and 302 W m^{-2}, respectively.

Temperature differences show strong mid–upper-level warming throughout development, with periods of weak cooling at low levels (Figure 14(c)). As in the other cases studied, the cooling is presumably associated with precipitation from deep convection, although, as noted earlier, the available analysis data are inadequate to confirm this result. The relative humidity in the column is generally high, mostly exceeding 85% throughout the period shown. Again, there is no indication of any appreciable intrusion of dry air into the inner core of the vortex. Throughout the troposphere, values of θ_e are the lowest of all three systems in this study and, at low levels, values remain relatively low (no

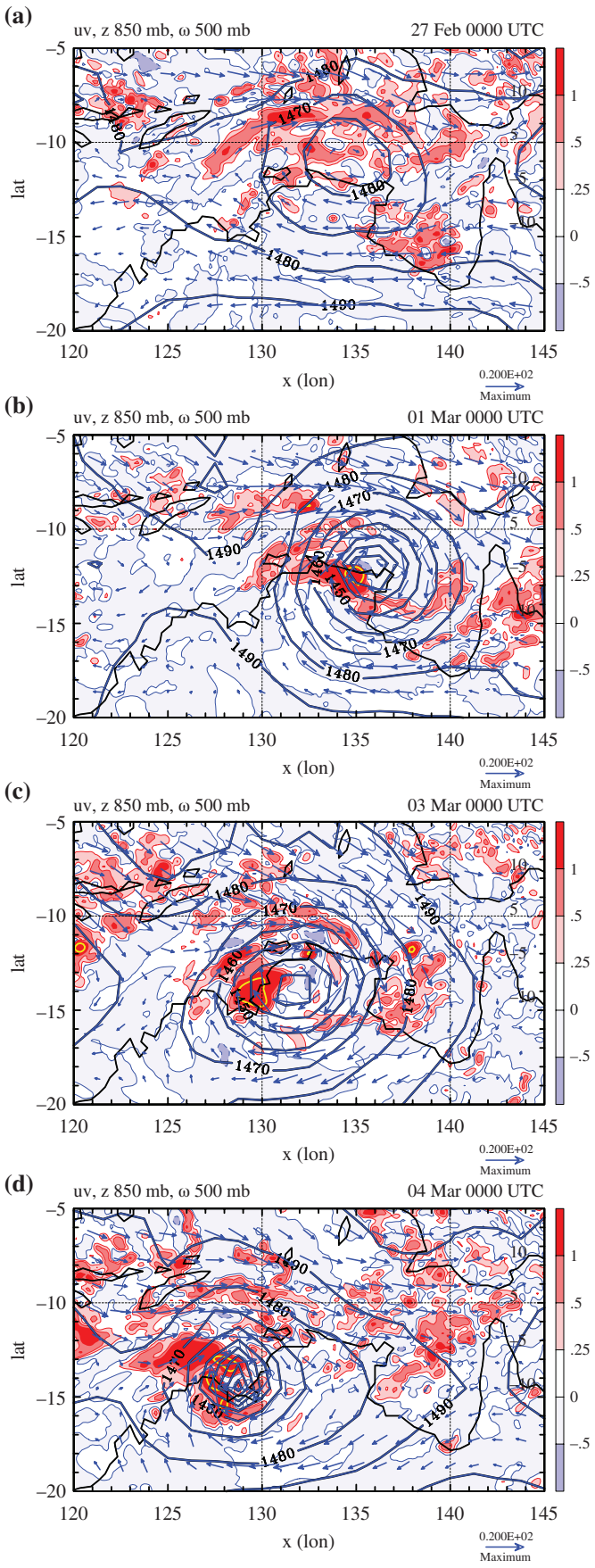

Figure 9. Wind vectors and contours of geopotential height, together with contours of the vertical velocity at 500 mb, at 0000 UTC on several days in February and March 2007, illustrating the formation of the low that became Tropical Cyclone *George*. The contour interval for geopotential height is 10 m. Vertical p velocity ($-\omega$) shading is as shown on the label bar in units Pa s^{-1}. Upward vertical velocities (negative values of ω) are plotted as positive (red/pink shading); negative values of vertical velocity (positive values of ω) as negative (light blue/blue shading). Strong regions of upflow are highlighted by the yellow contour (-2 Pa s^{-1}). Solid contours are positive, dashed contours negative. Wind vectors should be compared with the reference vector (20 m s^{-1}) at the bottom right of each panel.

dark red shading) in the low–mid-troposphere until 21 February. However, there are regular periods where θ_e is elevated at low levels to maintain convective instability.

The stronger bursts of deep convection (mass-flux values greater than 10×10^{-2} kg s^{-1} m^{-2}) that occur on 15 February and then again on 22 and 23 February are associated with increases in the circulation strength. The circulation around the 2°lon × 2°lat column begins to increase at low levels following these convective bursts. After the initial strong burst on 15 February, the circulation weakens and remains moderate until 21 February, when the low moves out over the water.

In summary, the low that became *Carlos* experienced an environment with initially low values of θ_e throughout the troposphere. There was relatively weak vertical shear before 15 February, although the shear increased in strength between 15 and 17 February, then subsequently decreased after that. During periods of relatively favourable vertical shear the system intensified, while it weakened during periods of unfavourable vertical shear. The circulation strength increased after a period of strong deep convective bursts near the circulation centre. Following these strong convective bursts was a period where the vertical mass-flux profile was consistently positive through much of the troposphere. During this period the circulation remained relatively constant. Later, strong deep convection occurred again and the system circulation increased in strength also.

6. Discussion

The mechanisms proposed here build on the work of tropical cyclogenesis by Dunkerton *et al.* (2009), Montgomery *et al.* (2012) and Smith and Montgomery (2012) (and references therein). The mechanisms share some similarity with the ideas of Raymond *et al.* (2014), in the sense of acknowledging the importance of a protected region that supports sustained vortex-tube stretching and upscale growth. However, Raymond *et al.* (2014) emphasize a thermodynamic control viewpoint, in which the vorticity dynamics in the early stages is basically slaved to the thermodynamic structure within the pouch region. They argue that a distinct middle-level (near 500 hPa) cyclonic vortex on a sub-synoptic scale and its associated cold core in the lower troposphere are crucial for supporting the transition from a top-heavy to a bottom-heavy convective mass-flux profile. However, we do not find the middle levels spinning up first, a commonly supposed prerequisite for cyclogenesis (see Figures 5(f), 10(f) and 14(f)). These results suggest the non-essential role of a distinct mid-level vortex in the low formation process in the ECMWF analyses.

The location of the monsoon shear line over the Australian continent increases the likelihood of low-pressure systems forming and intensifying over land. The question arises: do such developments differ appreciably from those for which the shear line is located over the sea? A comparison of the three lows examined here with the two systems analyzed by Smith *et al.* (2015) that developed over the sea suggests that the answer is no. In terms of vorticity dynamics, the processes appear to be just the same. Simply, as in Smith *et al.* (2015), patches of low-level, convectively enhanced vorticity in the vicinity of the monsoon shear line are converged by the broad-scale overturning circulation induced by clusters of deep convection. Above the frictional boundary layer, this convergence increases the circulation about fixed circuits encircling or within the convective region, thereby increasing the tangential wind component along that circuit. Since the absolute circulation and absolute angular momentum are proportional to one another, the process is equivalent (in an axisymmetric sense) to spin-up by the inward advection of surfaces of absolute angular momentum, sometimes referred to as the conventional, or classical, mechanism for spin-up articulated by Ooyama (1969): see the reviews by Montgomery and Smith (2014, 2017).

In both types of development, the broad-scale convectively induced convergence brings moisture into the system approximately equal to the loss of moisture by precipitation. In

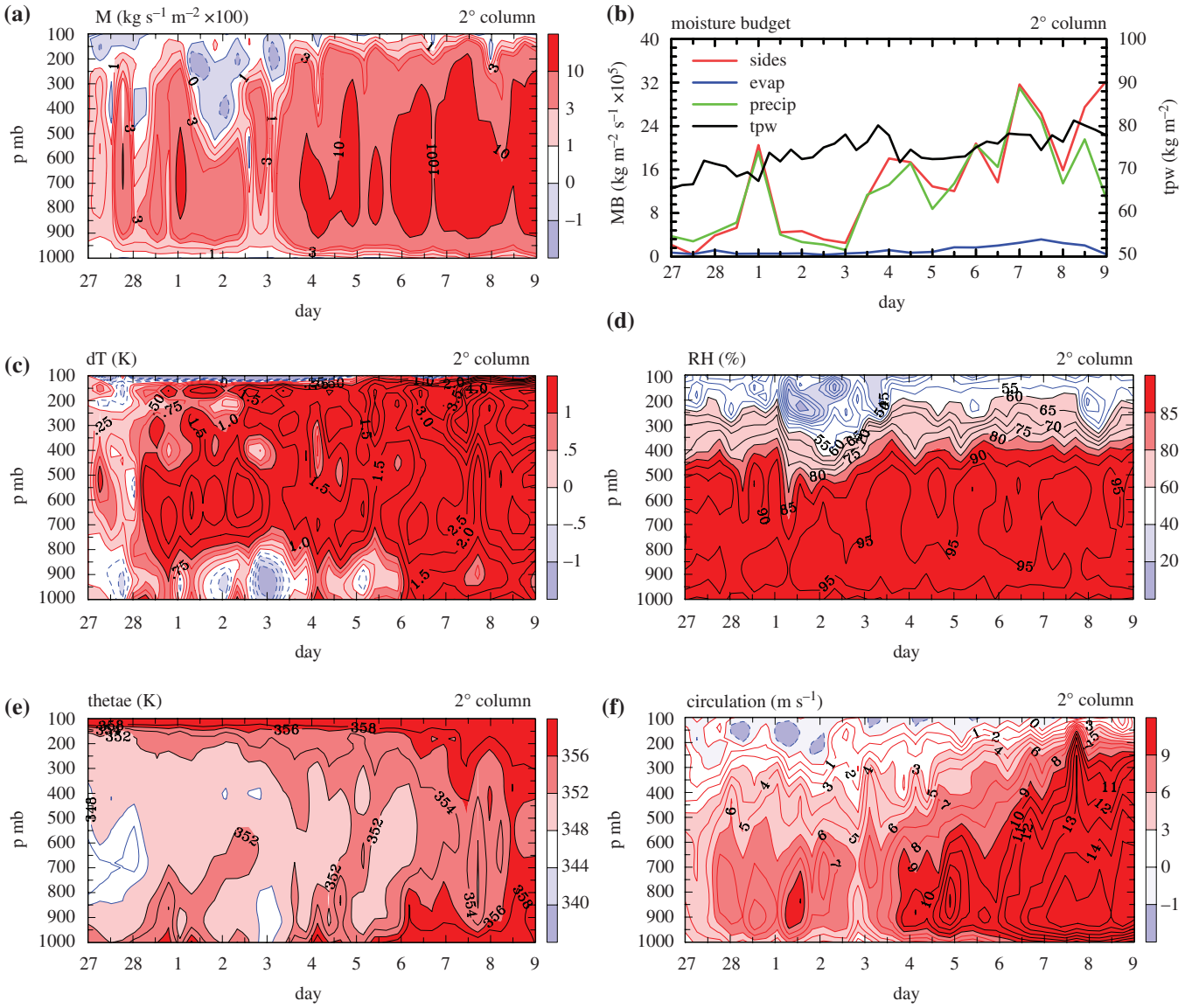

Figure 10. Time–height cross-section of system-averaged quantities within a column 2°lon × 2°lat, centred on the location of the minimum geopotential at 850 mb, for the development of the low that became Tropical Cyclone *George*. The panels have the same descriptions as those in Figure 5.

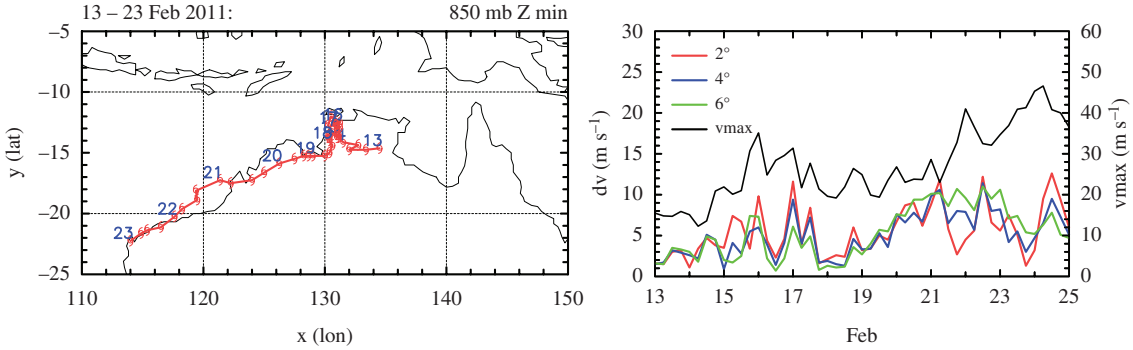

Figure 11. (a) Track of Tropical Cyclone *Carlos* in the Northern Territory region during the period 12–28 February 2011. Positions of minimum geopotential at 850 mb are indicated by cyclone symbols every 6 h. Positions at 0000 UTC are shown by date. (b) Mean vertical wind shear, characterized by the magnitude of the vector velocity difference between 850 and 200 mb, averaged over columns 2°lon × 2°lat, 4°lon × 4°lat and 6°lon × 6°lat centred on the location of the minimum geopotential at 850 mb, and maximum wind speed at 850 mb within the 2°lon × 2°lat column.

comparison, the supply of moisture at the surface is a small fraction of the total moisture budget. Nevertheless, the surface moisture flux is essential to maintain convective instability so that deep convection in the inner core region of the low can be sustained. The maintenance of instability over land is evidenced in the analyses by regular increases in low-level θ_e.

The main difference between systems that develop over land and those that develop over the sea is the more restricted supply of surface moisture (typically 100–150 W m^{-2} maximum during the daytime, compared with up to 700 W m^{-2} over the sea) and, of course, the larger friction over land. In this context, it is worth noting that, in a numerical modelling study, Montgomery *et al.* (2009) found that values of the order of 130 W m^{-2} are sufficient to support some degree of vortex intensification.

The present analyses, together with those of Kilroy *et al.* (2016) and the convection-permitting numerical simulations of Tang *et al.* (2016), indicate that levels of total precipitable water in the monsoon environment are high, even when the monsoon shear

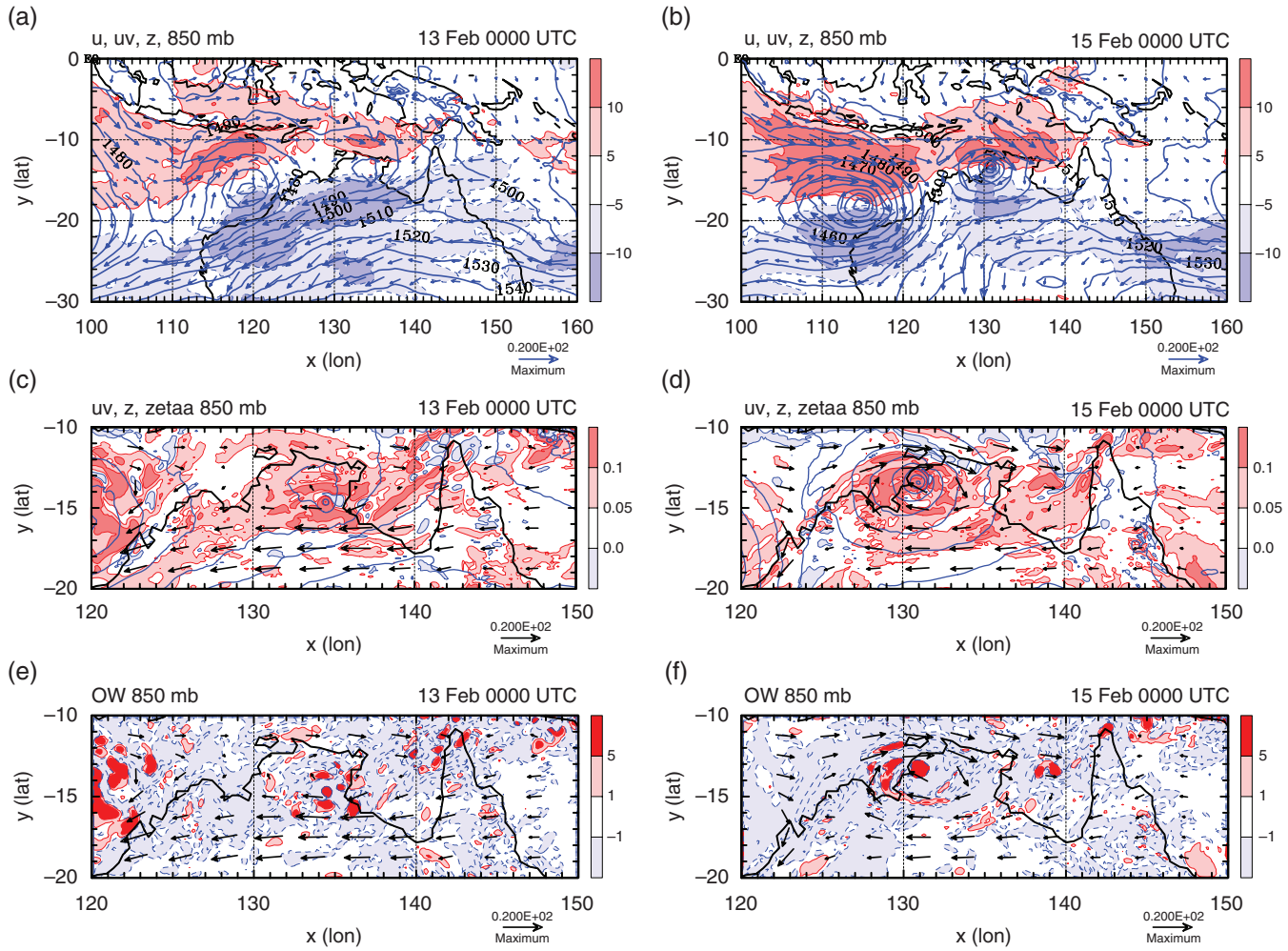

Figure 12. Wind vectors at 850 mb, together with contours of the zonal wind component and geopotential height, at 0000 UTC on (a) 13 February and (b) 15 February 2011. Contours are the same as in Figures 2 and 7. Wind vectors at 850 mb, together with contours of the absolute vorticity (shaded) and geopotential height (thick blue contours), at 0000 UTC on (c) 13 February and (d) 15 February 2011. Contours are the same as in Figures 3 and 8, left panels. Contours of the Okubo–Weiss (OW) parameter (shaded) at 0000 UTC on (e) 13 February and (f) 15 February 2011. Contours are the same as in Figures 3 and 8, right panels. Note the different latitude and longitude scales in (a) and (b) compared with (c)–(f).

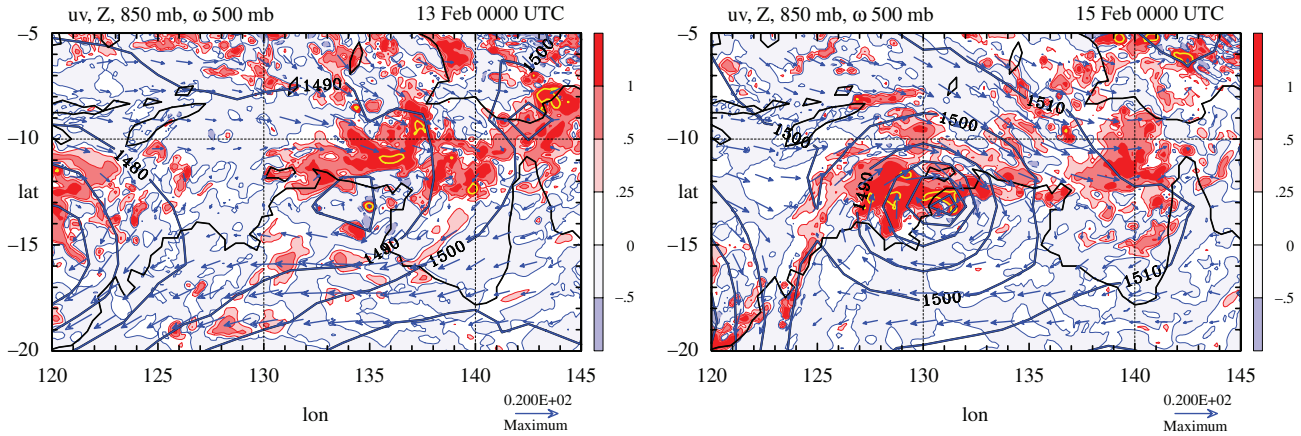

Figure 13. Wind vectors and contours of geopotential height, together with contours of the vertical velocity at 500 mb, at 0000 UTC on 13 and 15 February 2011, illustrating the formation of Tropical Cyclone *Carlos*. The contour interval for geopotential height is 10 m. Vertical p velocity ($-\omega$) shading is as shown on the label bar in units of Pa s^{-1}. Upward vertical velocities (negative values of ω) are plotted as positive (red/pink shading); negative values of vertical velocity (positive values of ω) as negative (light blue/blue shading). Strong regions of upflow are highlighted by the yellow contour (-2 Pa s^{-1}). Solid contours are positive, dashed contours negative. Wind vectors should be compared with the reference vector (20 m s^{-1}) at the bottom right of each panel.

line is over land. Thus, in the absence of appreciable vertical shear, the moist monsoonal environment locally surrounding the storm provides a shield against the adverse effects of dry-air intrusion from the Australian continent.

In summary, echoing the previous results of Smith *et al.* (2015), Kilroy *et al.* (2016) and Tang *et al.* (2016), the results of this study would suggest that the processes of tropical low formation and intensification over land are *not* fundamentally different from those over the sea. In essence, tropical lows in a monsoon environment are warm-cored, convectively driven vortices just like tropical cyclones.

7. Conclusions

In continuation of recent studies on the same topic, we have presented an analysis of tropical low formation and intensification

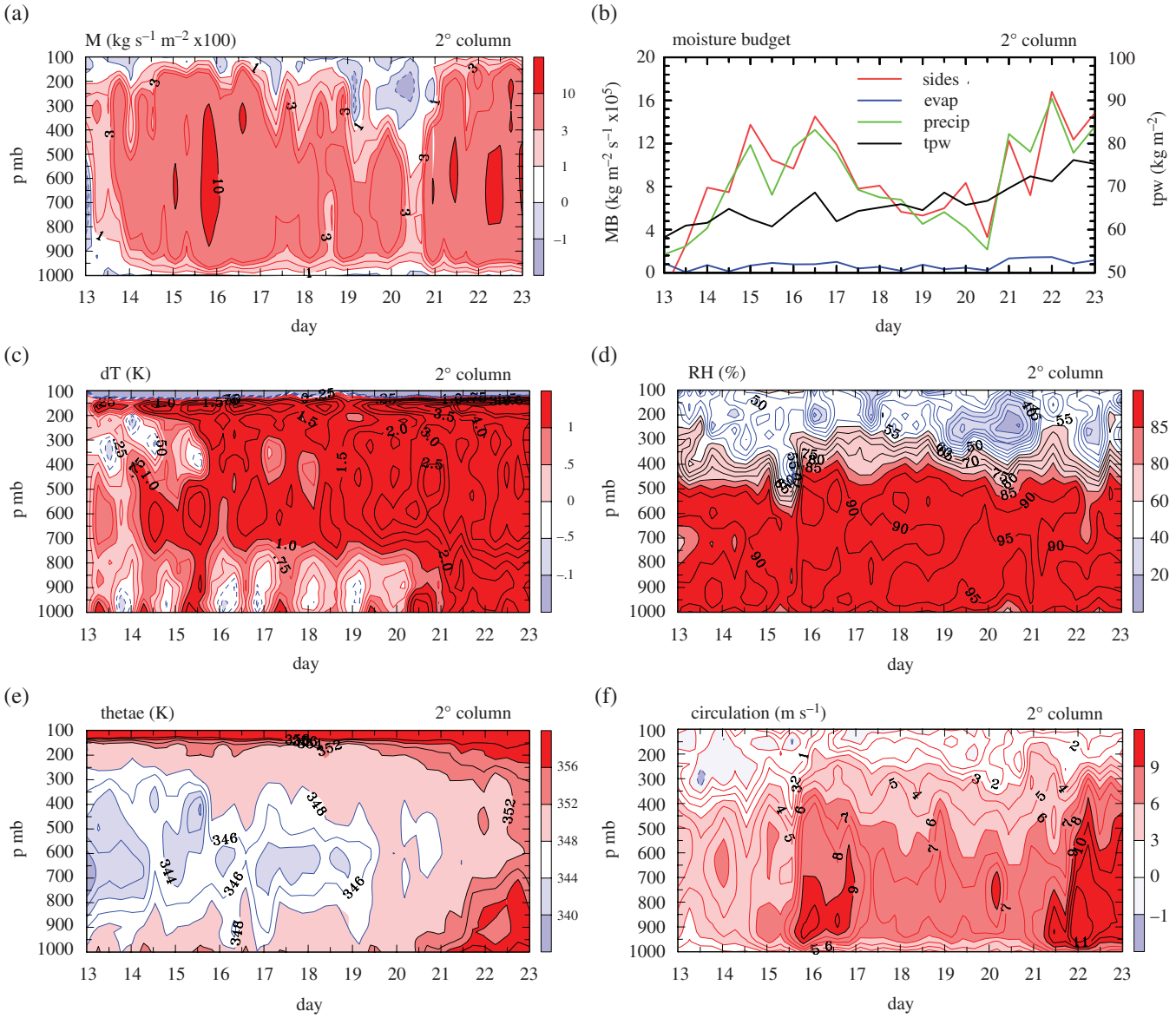

Figure 14. Time–height cross-section of system-averaged quantities within a column 2°lon × 2°lat, centred on the location of the minimum geopotential at 850 mb, for the development of the low that became Tropical Cyclone *Carlos*. The panels have the same descriptions as those in Figure 5.

over land during the Australian monsoon, based on ECMWF analyses. In particular, we examined three lows (2006, 2007, 2011) that developed and intensified either over land or near the coast. The findings point to the generality of those in earlier studies and identify processes that are canonical in low development.

- The analyses highlight a need for the occurrence of repeated bursts of deep convection near the nascent circulation centre. The inflow in the lower troposphere accompanying the convectively induced overturning circulation concentrates cyclonic vorticity, thereby increasing the circulation about the vortex centre as well as the local tangential wind speed. On the assumption that, above the boundary layer, there is approximate gradient wind balance, the increase in tangential wind speed corresponds to a lowering of the central pressure. If deep convection diminishes (i.e. the convective mass flux declines), the low weakens progressively.
- The convectively induced inflow in the lower troposphere imports air into the low from its moist monsoonal environment. This moist monsoonal environment locally surrounding the storm provides a shield against the adverse effects of dry-air intrusion from the Australian continent.
- In terms of a moisture budget, surface fluxes of moisture are small in comparison with the convergence of environmental moisture, but, as for lows that form over the sea, these surface fluxes are important in maintaining convective instability near the vortex centre. In essence, the processes of intensification are the same over land as those that operate over the ocean. Even though the surface moisture fluxes are larger when the low is located over the sea, the fluxes over land during the monsoon are large enough to support persistent deep convection near the circulation centre. However, they are not large enough to allow storms to achieve more than minimal tropical cyclone intensity, in part because of the increased surface friction over land.

The results of this study and its companions suggest the application of the diagnostic tools developed here as a means to help forecasters with these types of development.

Acknowledgements

We thank Timothy W. Cronin and an anonymous reviewer for their careful reading and their perceptive comments on the original manuscript. GK and RKS acknowledges funding for tropical cyclone research from the German Research Council (Deutsche Forschungsgemeinschaft) under Grant no SM30/23-4 and the Office of Naval Research Global under Grant No. N62909-15-1-N021. MTM acknowledges the support of NSF grant AGS-1313948, NOAA HFIP grant N0017315WR00048, NASA grant NNG11PK021 and the US Naval Postgraduate School.

References

Bauer P, Auligné T, Bell W, Geer A, Guidard V, Heilliette S, Kazumori M, Kim M-J, Liu EH-C, McNally AP, Macpherson B, Okamoto K, Renshaw R, Riishøjgaard L-P. 2011. Satellite cloud and precipitation assimilation at operational NWP centres. *Q. J. R. Meteorol. Soc.* **137**: 1934–1951.

Davidson NE, Holland GH. 1987. A diagnostic analysis of two intense monsoon depressions over Australia. *Mon. Weather Rev.* **115**: 380–392.

DeMaria M, Kaplan J. 1994. A statistical hurricane intensity prediction scheme (SHIPS) for the Atlantic basin. *Weather and Forecasting* **9**: 209–220.

Dunkerton TJ, Montgomery MT, Wang Z. 2009. Tropical cyclogenesis in a tropical wave critical layer: easterly waves. *Atmos. Chem. Phys.* **9**: 5587–5646.

Foster IJ, Lyons TJ. 1984. Tropical cyclogenesis: A comparative study of two depressions in the northwest of Australia. *Q. J. R. Meteorol. Soc.* **110**: 105–119.

Hendricks EA, Montgomery MT, Davis CA. 2004. On the role of 'vortical' hot towers in formation of Tropical Cyclone *Diana* (1984). *J. Atmos. Sci.* **61**: 1209–1232.

Kilroy G, Smith RK, Montgomery MT, Lynch B, Earl-Spurr C. 2016. A case study of a monsoon low that formed over the sea and intensified over land as seen in the ECMWF analyses. *Q. J. R. Meteorol. Soc.* **142**: 2244–2255.

McBride JL, Keenan TD. 1982. Climatology of tropical cyclone genesis in the Australian region. *J. Clim.* **2**: 13–33.

May PT, Mather JH, Vaughan G, Jakob C. 2008a. Characterizing oceanic convective cloud systems. *Bull. Am. Meteorol. Soc.* **89**: 153–155.

May PT, Mather JH, Vaughan G, Jakob C, McFarquhar GM, Bower KN, Mace GG. 2008b. The tropical warm pool international cloud experiment. *Bull. Am. Meteorol. Soc.* **89**: 153–155.

Montgomery MT, Smith RK. 2014. Paradigms for tropical-cyclone intensification. *Aust. Meteorol. Oceanogr. J.* **64**: 37–66.

Montgomery MT, Smith RK. 2017. Recent developments in the fluid dynamics of tropical cyclones. *Annu. Rev. Fluid Mech.* **49**: 1–33, doi: 10.1146/annurev-fluid-010816-060022.

Montgomery MT, Nicholl ME, Cram TA, Saunders A. 2006. A 'vortical' hot tower route to tropical cyclogenesis. *J. Atmos. Sci.* **63**: 355–386.

Montgomery MT, Nguyen SV, Smith RK, Persing J. 2009. Is WISHE essential for tropical cyclone intensification? *Q. J. R. Meteorol. Soc.* **135**: 1697–1714.

Montgomery MT, Davis C, Dunkerton T, Wang Z, Velden C, Torn R, Majumdar SJ, Zhang F, Smith RK, Bosart L, Bell MM, Haase JS, Heymsfield A, Jensen J, Campos T, Boothe MA. 2012. The Pre-Depression Investigation of Cloud Systems in the Tropics (PREDICT) experiment: Scientific basis, new analysis tools and some first results. *Bull. Am. Meteorol. Soc.* **93**: 153–172.

Nolan DS. 2007. What is the trigger for tropical cyclogenesis? *Aust. Meteorol. Mag.* **56**: 241–266.

Ooyama KV. 1969. Numerical simulation of the life cycle of tropical cyclones. *J. Atmos. Sci.* **26**: 3–40.

Raymond DJ, López Carillo C. 2011. The vorticity budget of developing typhoon *Nuri* (2008). *Atmos. Chem. Phys.* **11**: 147–163.

Raymond DJ, Gjorgjievska S, Sessions SL, Fuchs Z. 2014. Tropical cyclogenesis and mid-level vorticity. *Aust. Meteorol. Oceanogr. Soc. J.* **64**: 11–25.

Smith RK, Montgomery MT. 2012. Observations of the convective environment in developing and non-developing tropical disturbances. *Q. J. R. Meteorol. Soc.* **138**: 1721–1739.

Smith RK, Montgomery MT, Kilroy G, Tang S, Müller SK. 2015. Tropical low formation during the Australian monsoon: The events of January 2013. *Aust. Meteorol. Oceanogr. Soc. J.* **65**: 318–341.

Tang S, Smith RK, Montgomery MT, Gu M. 2016. Numerical study of the spin up of a tropical low over land during the Australian monsoon. *Q. J. R. Meteorol. Soc.* **142**: 2021–2032.

Tory KJ, Montgomery MT, Davidson NE. 2006a. Prediction and diagnosis of tropical cyclone formation in an NWP system. Part I: The critical role of vortex enhancement in deep convection. *J. Atmos. Sci.* **63**: 3077–3090.

Tory KJ, Montgomery MT, Davidson NE, Kepert JD. 2006b. Prediction and diagnosis of tropical cyclone formation in an NWP system. Part II: A detailed diagnosis of tropical cyclone *Chris* formation. *J. Atmos. Sci.* **63**: 3091–3113.

Tory KJ, Davidson NE, Montgomery MT. 2007. Prediction and diagnosis of tropical cyclone formation in an NWP system. Part III: Diagnosis of developing and nondeveloping storms. *J. Atmos. Sci.* **64**: 3195–3213.

